

Enhancement of wave damping within metamaterials having embedded negative stiffness inclusions

D. Chronopoulos^a, I. Antoniadis^b, M. Collet^c, M. Ichchou^d

^a*Division of Materials, Mechanics and Structures, University Park, The University of Nottingham, NG7 2RD, UK*

^b*Machine Design and Control Systems Section, School of Mechanical Engineering, National Technical University of Athens, Greece*

^c*LTDS, UMR-CNRS 5513, 36 Avenue Guy de Collongue, 69130 Ecully, France*

^d*Ecole Centrale de Lyon, 36 Avenue Guy de Collongue, 69130 Ecully, France*

Abstract

The wave dissipation properties of layered periodic structures are modelled by FE as well as analytical approaches. A linear oscillator incorporating a negative stiffness element and having exceptional energy dissipation properties is exhibited and incorporated within the modelled structures. The structural dynamic stability of both the oscillator and the modelled waveguides is discussed and ensured. The numerical results provide evidence of a drastic increase of several orders of magnitude for the damping ratio of the flexural waves propagating within the structures.

Keywords: Damping, Negative Stiffness, Composite Structures, Metamaterials, Wave Propagation

1. Introduction

The need of cost and mass efficient vibration isolation within the modern aerospace, automotive and civil industries has been a particularly intense subject of research during the last decades. For the space industry it is crucial to prevent damage to the payload and the spacecraft structures during launch. Aircraft structures are facing similar challenges with the cabin interior noise levels being one of the major quality criteria for modern aircrafts, while in the automotive industry there is also a growing interest to isolate the nuisance induced by the road surface roughness and the power-train system from the passenger compartment.

The current perception is that damping is produced by physical mechanisms generating energy dissipation in an oscillating system, such as friction, hysteresis, drag, hydraulic and electrical resistance, etc. The dominant engineering practice for increasing structural damping is the usage of dissipative (mostly viscoelastic) materials [1, 2]. Current dissipative materials are characterized by moderate to low stiffness, which renders them unsuitable for demanding load carrying applications [3]. Despite being of generally low mass density, the volume of dissipative materials that has to be used renders their application prohibitive for moving structures. Moreover it has been demonstrated [4, 5] that within a layered structure the impact of the damping of a single layer on the total damping factor of the structure is proportional to the flexural stiffness of the layer (proportional to the deformation energy stored in the layer); thus

Email address: Dimitrios.Chronopoulos@nottingham.ac.uk (D. Chronopoulos)

suggesting that for composite structures comprising stiff, carbon fibre containing layers, the effect of the damping factor of a viscoelastic layer will inevitably be alleviated.

However, possibilities towards achieving significant damping have been identified in materials comprising a negative stiffness phase [6, 7]. Quite interestingly, such a behavior is combined with high stiffness properties. The fact that structures with negative stiffness perform satisfactorily in certain types of shock and vibration damping engineering applications has been studied for some time and a comprehensive review of such applications can be found in [8]. The negative stiffness behavior is shown to result actually in special mechanical designs involving conventional positive stiffness prestressed elastic mechanical elements, such as 'snap-through' designs, or post-buckled beams. Quite recently, the authors in [9, 10] have shown that inclusion of negative-stiffness phases within elastic composites can only induce an elevated stiffness in a dynamic sense. Periodic cellular structures have been also proposed [11, 12, 13, 14, 15] with pronounced damping properties, combining high positive and negative stiffnesses. Although the physical mechanisms that generate pronounced damping in cellular structures are not profoundly understood, microbuckling or slip-stick phenomena [16, 17, 18] are among the possible explanations.

With regard to the design of engineering structures where vibration damping is achieved by the use of discrete macroscopic elements, such as springs and dampers. It should be noted that the concept of introducing negative stiffness elements (or 'anti-springs') for vibration isolation has a long history, being introduced in the pioneering publication of [19] as well as in the milestone developments [20, 21]. A rich variety of designs has been proposed for the realisation of negative spring configurations, incorporating various structural elements such as post-buckled beams, plates, shells and precompressed springs, arranged in appropriate geometrical configurations. Some interesting designs are described in [22, 23, 24, 25, 26, 27]. The central concept of these approaches is to significantly reduce the stiffness of the isolator and consequently of the natural frequency of the system even at almost zero levels [28]. In this way, the transmissibility of the system for all operating frequencies above the natural frequency is reduced, resulting to enhanced vibration isolation. An initial comprehensive review of such designs can be found in [29]. Since then, numerous other applications have been reported in a diversity of engineering domains, such as automotive suspensions [30, 31, 32] or seismic isolation [33, 34]. From the fundamental design point of view, many interesting improvements have been proposed, based on the non-linear properties of the elastic force of such designs [35, 36, 37, 38, 39]. However, all these designs suffer from their fundamental requirement for a drastic reduction of the stiffness of the structure almost to negligible levels, limiting thus the static load capacity of such structures.

In this paper the design of a stable oscillator comprising negative stiffness elements is initially exhibited and results on its dynamic response are presented. The results suggest a radical increase of the oscillator's inherent damping ratio. The suggested oscillator is then implemented in two structural configurations: i) An elastically supported continuous beam structure which is analytically modelled and ii) A periodic layered beam structure which is modelled using FE. The damping ratio for each wave type propagating within the two modelled configurations is computed. The numerical results provide evidence of a drastic increase of several orders of magnitude for the damping ratio of the waves propagating within the structures when the suggested configuration comprising negative stiffness inclusions is

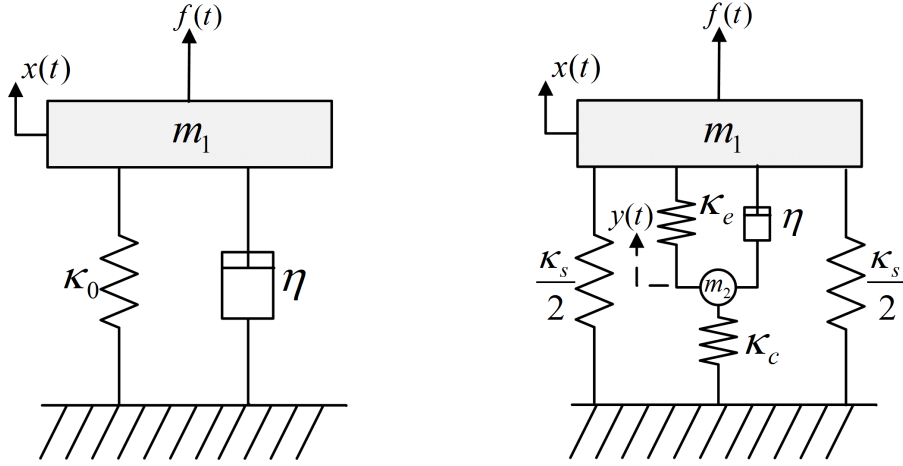


Figure 1: Left: A typical (reference) SDOF dynamic system consisting of a mass m , a stiffness κ_0 and a dashpot η . The system exhibits a natural frequency ω_0 and a damping ratio ζ_0 . Right: The proposed configuration, resulting from the reference SDOF system, after the proper redistribution of the stiffness, the reallocation of the damping element and the addition of m_2 as a result of introducing the negative stiffness mechanism. Both systems have the same (static) stiffness under Eq.1.

implemented.

The paper is organized as follows: In Sec.2 a description is given for the design of the unit cell oscillator having negative stiffness inclusions. In Sec.3 a continuous beam structure, supported by stiffness and dissipation elements on an undeformable floor is modelled. The suggested unit cell oscillator is then implemented in the system and the damping ratio of the propagating flexural waves are computed and compared before and after the implementation of the oscillator. In Sec.4 a periodic layered structure is modelled using FE and the characteristics of the propagating acoustic waves are sought using periodic structure theory. Once again the suggested oscillator is incorporated within the system and the results on the flexural wave dissipation properties are computed in Sec.5. Conclusions on the presented work are eventually drawn in Sec.6.

2. The proposed configuration having a negative stiffness inclusion

The proposed configuration with a stable negative stiffness inclusion κ_c is introduced in Fig.1.

2.1. Dynamic analysis

It is actually a linear stable oscillator, designed in such a way that it has a static stiffness κ_0 which is the same to the one of the reference SDOF oscillator (also in Fig.1).

$$\kappa_s + \frac{\kappa_e \kappa_c}{\kappa_e + \kappa_c} = \kappa_0 \quad (1)$$

An additional mass m_2 is included in the modified oscillator to take into account for the additional weight implied by the introduction of the negative stiffness mechanism. A variety of choices exists for realizing the negative stiff-

ness, including post-buckled elements [40] and negative impedance piezoelectric circuits [41]. The two systems also comprise the same damping element of coefficient η . The equations of motion for the DoF x, y of the modified system illustrated in Fig.1 can be written as

$$m_1 \ddot{x} + \eta(\dot{x} - \dot{y}) + \kappa_s x + \kappa_e(x - y) = f \quad (2a)$$

$$m_2 \ddot{y} + \eta(\dot{y} - \dot{x}) + \kappa_e(y - x) + \kappa_c y = 0 \quad (2b)$$

with f being the external excitation applied to the 'apparent' DoF x . By introducing Eq.2b in 2a and applying a Laplace transform the above system of equations can be expressed as

$$Y = \frac{s\eta + \kappa_e}{s^2 m_2 + s\eta + \kappa_e + \kappa_c} X \quad (3a)$$

$$X = \frac{s^2 m_2 + s\eta + \kappa_e + \kappa_c}{(s^2 m_1 + s\eta + \kappa_e + \kappa_s)(s^2 m_2 + s\eta + \kappa_e + \kappa_c) - (s\eta + \kappa_e)^2} F \quad (3b)$$

which results in

$$Y = \frac{s\eta + \kappa_e}{b_2 s^2 + b_1 s + b_0} X \quad (4a)$$

$$X = \frac{s^2 m_2 + s\eta + \kappa_e + \kappa_c}{c_4 s^4 + c_3 s^3 + c_2 s^2 + c_1 s + c_0} F \quad (4b)$$

with

$$b_2 = m_2 \quad (5a)$$

$$b_1 = \eta \quad (5b)$$

$$b_0 = \kappa_e + \kappa_c \quad (5c)$$

and

$$c_4 = m_1 m_2 \quad (6a)$$

$$c_3 = \eta(m_1 + m_2) \quad (6b)$$

$$c_2 = m_1(\kappa_c + \kappa_e) + m_2(\kappa_e + \kappa_s) \quad (6c)$$

$$c_1 = \eta(\kappa_c + \kappa_s) \quad (6d)$$

$$c_0 = \kappa_s(\kappa_e + \kappa_c) + \kappa_e \kappa_c \quad (6e)$$

The stability of the proposed configuration is subsequently discussed.

2.2. Design of a stable oscillator

The authors in [42] have shown that lumped parameter oscillators with negative system inclusions can be stable. By applying a Routh-Hurwitz stability criterion it is derived that the necessary and sufficient conditions for the stability of the oscillator proposed in this work are

$$b_0 > 0 \Leftrightarrow m_2 > 0 \quad (7a)$$

$$b_1 > 0 \Leftrightarrow \eta > 0 \quad (7b)$$

$$b_2 > 0 \Leftrightarrow \kappa_e + \kappa_c > 0 \quad (7c)$$

as well as

$$c_0 > 0 \Leftrightarrow \kappa_s(\kappa_e + \kappa_c) + \kappa_e\kappa_c > 0 \quad (8a)$$

$$c_1 > 0 \Leftrightarrow \eta(\kappa_c + \kappa_s) > 0 \quad (8b)$$

$$c_2 > 0 \Leftrightarrow m_1(\kappa_c + \kappa_e) + m_2(\kappa_e + \kappa_s) > 0 \quad (8c)$$

$$c_3 > 0 \Leftrightarrow \eta(m_1 + m_2) > 0 \quad (8d)$$

$$c_4 > 0 \Leftrightarrow m_1m_2 > 0 \quad (8e)$$

$$c_3c_2 > c_4c_1 \Leftrightarrow \kappa_cm_1^2 + \kappa_em_1^2 + \kappa_em_2^2 + \kappa_sm_2^2 + 2\kappa_em_1m_2 > 0 \quad (8f)$$

$$c_3c_2c_1 > c_4c_1^2 + c_3^2c_0 \Leftrightarrow \eta^2(\kappa_cm_1 - \kappa_sm_2)^2 > 0 \quad (8g)$$

It is evident that Eq.7a, 7b, 8d, 8e and 8g are a priori satisfied. Satisfaction of Eq.7c implies that Eq.8c should also be valid. Moreover if Eq.8a is true, Eq.7c is also satisfied. The stability conditions for the system are therefore acquired by Eq.8a, 8b and 8f. Eq.8f can be expressed as

$$\kappa_c > -\kappa_e \left(1 + \left(\frac{m_2}{m_1} \right)^2 + 2 \frac{m_2}{m_1} \right) - \kappa_s \left(\frac{m_2}{m_1} \right)^2 \quad (9)$$

However $\left(1 + \left(\frac{m_2}{m_1} \right)^2 + 2 \frac{m_2}{m_1} \right) > 1$ and in view of the above it is implied that if Eq.8a holds then Eq.9 is also satisfied, therefore static and dynamic stability for the oscillator is ensured by

$$\kappa_e + \kappa_c > \left| \frac{\kappa_e\kappa_c}{\kappa_s} \right| \quad (10a)$$

$$\kappa_s > -\kappa_c \quad (10b)$$

The oscillator is designed so that an engineering tolerance (or safety margin) ε exists, prohibiting κ_c from reaching its limit value that would induce neutral static stability, therefore

$$\kappa_s + \frac{(1 + \varepsilon)\kappa_c\kappa_e}{(1 + \varepsilon)\kappa_c + \kappa_e} = 0 \quad (11)$$

It is also assumed that

$$\kappa_s = \alpha\kappa_0 \quad (12)$$

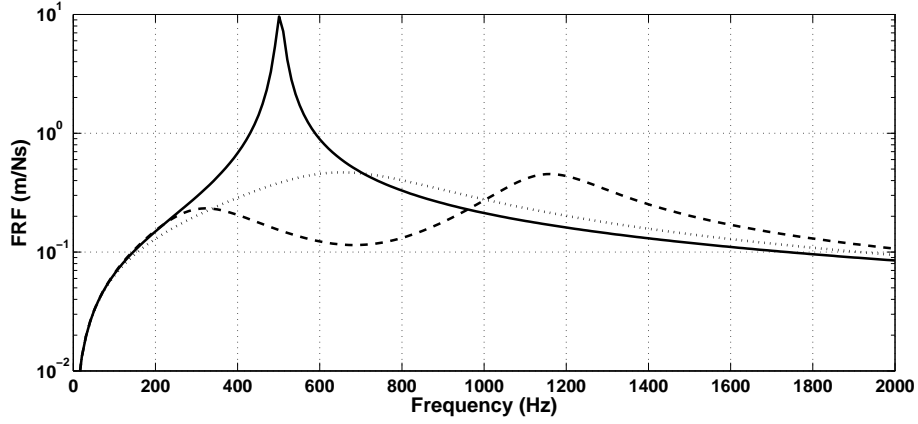


Figure 2: Comparison of the FRF V_x/F for: the SDOF system (—), the modified oscillator with $m_2=0$ (···) and the modified oscillator with $m_2=0.05m_1$ (- -). The design parameters of the system are $\varepsilon=5\%$ and $\alpha=3.3$ while $\eta=10\%$.

with α being the second design parameter. In view of Eq.1, 11 and 12 the stiffness elements κ_s , κ_c and κ_e of the proposed oscillator, are designed with relation to κ_0 of the original system, by the following set of equations

$$\kappa_s = \alpha\kappa_0 \quad (13a)$$

$$\kappa_e = \kappa_0 \frac{\varepsilon\alpha(\alpha - 1)}{1 + \varepsilon - \alpha\varepsilon} \quad (13b)$$

$$\kappa_c = -\kappa_0 \frac{\varepsilon\alpha(\alpha - 1)}{1 + \varepsilon} \quad (13c)$$

while simultaneously satisfying Eq.10 will ensure the stability of the system.

2.3. Numerical case study on the suggested oscillator design

The admittance Frequency Response Functions (FRF) V_x/F for the original SDOF system as well as for the oscillator having negative stiffness inclusions are presented in Fig.2. The parametric values for the SDoF oscillator are selected as: $\kappa_0 = 10^4$ N/m, $m = 10^{-3}$ kg and $\eta=0.1$. It is observed that when $\lim m_2 \rightarrow 0^+$ the response of the modified oscillator presents a significantly higher attenuation compared to the SDOF system and is reduced by a factor of 25 close to the original natural frequency ω_0 of the system. Beyond resonance, the response of the modified oscillator asymptotically converges towards the one of the SDOF system. When $m_2 > 0$ two resonance frequencies are observed for the modified system. The response V_x/F thus presents an antiresonance and is further reduced in the vicinity of ω_0 while it exhibits two local maxima at resonances ω_{n1}, ω_{n2} with the later being due to the addition of the mass m_2 .

One of the most important design objectives for the oscillator is maximizing its damping characteristics. The damping ratio ζ_n of the modified system can be calculated as a function of the poles of the characteristic equation of the system in Eq.4. The value of ζ_n for various values of the damping coefficient η of the dashpot element is shown in Fig. 3 The results are given as the ratio of ζ_n to the damping ratio of the SDoF system

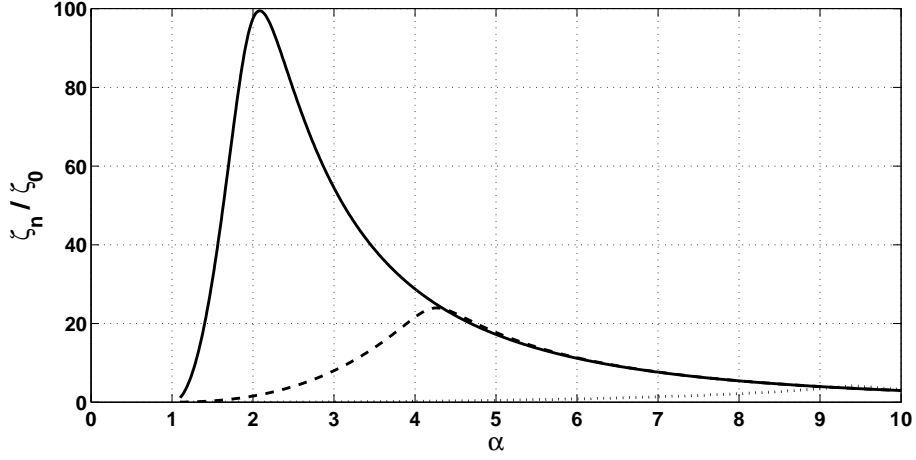


Figure 3: The impact of η on the damping ratio enhancement ζ_n/ζ_0 of the suggested oscillator with $m_2=0$: $\zeta_0=0.1$ (\cdots), $\zeta_0=0.01$ ($- -$), $\zeta_0=0.001$ ($-$). All computations conducted with $\varepsilon=5\%$.

$$\zeta_0 = \frac{\eta}{2\sqrt{m\kappa_0}} \quad (14)$$

It is observed that an optimal α value exists for any η that maximizes the damping ratio of the system. As expected, increasing η increases ζ_n ; however this increase is not linear as with the SDoF system. Taking a look at the maximum ζ_n values it is observed that increasing η by a factor of 100 will only increase the maximum ζ_n by a factor of 4. Comparing the maximum ζ_n values to ζ_0 it is observed that for $\zeta_0 = 1\%$ the damping ratio is amplified by a factor of 18, while for $\zeta_0 = 0.1\%$ the damping ratio is increased by up to a factor of 100. It can therefore be concluded that an impressive improvement of the damping capabilities takes place for the modified system; this improvement is greater for lightly damped systems.

3. Wave dissipation within a continuous beam structure

The first configuration under consideration will be a beam connected to an undeformable body (floor) through a stiffness κ_0 and a viscous damping element η as illustrated in Fig.4. The beam is made of a material having a Young's modulus equal to E and a mass per length ratio equal to M , while its second moment of area (around the bending neutral axis) is equal to I . Using the Euler-Bernoulli beam theory to model the structure (thus ignoring shear deformation and rotational inertia effects) the equation of motion for an infinitesimal part of the structure can be written as

$$EI \frac{\partial^4 w}{\partial x^4} + M \frac{\partial^2 w}{\partial t^2} + \eta \frac{\partial w}{\partial t} + \kappa_0 w = 0 \quad (15)$$

Assuming time harmonic wave motion within the infinite medium, the Bloch's theorem [43] can be employed in order to provide a generalized relation for the displacements as

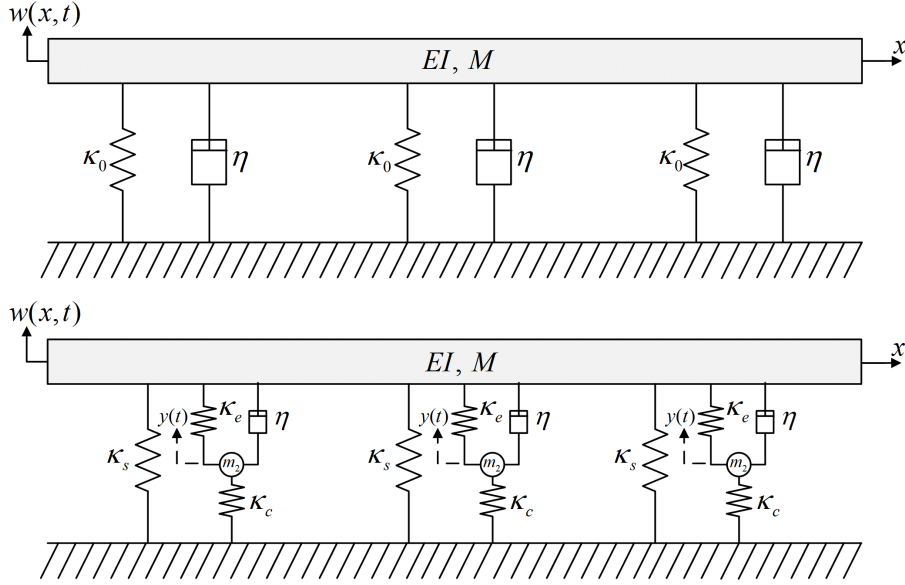


Figure 4: Illustration of an infinitesimal part of the considered beam. Top: The beam connected to the floor through a stiffness κ_0 and a damping coefficient η . Bottom: The beam connected to the floor using the suggested mechanism with η equal to the precedent case, κ_s, κ_e positive stiffness and κ_c negative stiffness elements.

$$w(x, t) = W e^{-ikx + \lambda t} \quad (16)$$

with W being the wave motion amplitude, x the longitudinal distance from the reference to the considered point on the structure, k represents the wavenumber and λ is a complex frequency function permitting time induced wave attenuation. In the absence of damping, $\lambda = \pm i\omega$ so that the usual form of Bloch's theorem is recovered. In the presence of damping the real part of λ represents the attenuation of the wave in which case

$$\lambda(k) = -\xi(k)\omega(k) \pm i\omega_d(k) \quad (17)$$

with ξ the damping ratio of the considered wave type and ω_d the frequency at which the assumed wavenumber value for the damped wave is occurring. Substituting Eq.16 into 15 a second order polynomial expression is obtained for λ is therefore obtained as

$$M\lambda^2 + \eta\lambda + EI k^4 + \kappa_0 = 0 \quad (18)$$

the solutions of which can provide the wavenumber dependent damping ratios for the flexural wave propagating within the considered system.

The 'beam on a floor' system incorporating the suggested negative stiffness inclusions is also illustrated in Fig.4. It should be stressed that the two systems presented in the figure are statically equivalent. The equations for the vertical motion of the beam w and the internal DoF y can be written again using an Euler-Bernoulli approach as

$$EI \frac{\partial^4 w}{\partial x^4} + M \frac{\partial^2 w}{\partial t^2} + \eta \left(\frac{\partial w}{\partial t} - \frac{\partial y}{\partial t} \right) + \kappa_e (w - y) + \kappa_s w = 0 \quad (19a)$$

$$m_2 \frac{\partial^2 y}{\partial t^2} + \eta \left(\frac{\partial y}{\partial t} - \frac{\partial w}{\partial t} \right) + \kappa_e (y - w) + \kappa_c y = 0 \quad (19b)$$

The Bloch's theorem is engaged to provide a generalized relation for the displacements as

$$w(x, \lambda, t) = W e^{-ikx + \lambda t} \quad (20a)$$

$$y(x, \lambda, t) = Y e^{-ikx + \lambda t} \quad (20b)$$

with W, Y being the wave motion amplitudes. Introducing Eq.20 into 19b can provide an expression for the relation of W, Y as

$$\begin{aligned} m_2 \lambda^2 Y e^{-ikx + \lambda t} + \eta (\lambda Y e^{-ikx + \lambda t} - \lambda W e^{-ikx + \lambda t}) + \kappa_e (Y e^{-ikx + \lambda t} - W e^{-ikx + \lambda t}) + \kappa_c Y e^{-ikx + \lambda t} = 0 \Rightarrow \\ \Rightarrow Y = \frac{\kappa_e + \lambda \eta}{m_2 \lambda^2 + \eta \lambda + \kappa_c + \kappa_e} W \end{aligned} \quad (21)$$

while by substituting Eq.21 into 19a a fourth order polynomial expression is obtained for λ as

$$\begin{aligned} M m_2 \lambda^4 + (M + m_2) \eta \lambda^3 + (E I m_2 k^4 + M \kappa_c + M \kappa_e + \kappa_e m_2 + \kappa_s m_2) \lambda^2 + \\ + (E I k^4 + \kappa_c + \kappa_s) \eta \lambda + E I k^4 (\kappa_c + \kappa_e) + \kappa_c \kappa_e + \kappa_c \kappa_s + \kappa_e \kappa_s = 0 \end{aligned} \quad (22)$$

the solutions of which will provide the wavenumber dependent damping ratios for the waves propagating within the configuration comprising negative stiffness inclusions at κ_c .

4. Wave dissipation within a periodic layered structure

The second configuration to be considered is a layered beam structure comprising two facesheets and a core layer. In order to take into account for the impact of the core shear deformation to the acoustic wave propagation characteristics a periodic segment of the layered structure is modelled by FE. This would be rather complicated to capture using analytical methods [44]. An additional advantage of FE techniques over analytical approaches is that when it comes to modelling geometrically complex structures, the embedded FE 3D displacement functions ensure a more generic way of capturing the entirety of the propagating waves. The mass, damping and stiffness matrices of the segment \mathbf{M} , \mathbf{C} and \mathbf{K} are extracted using a conventional FE software. In the first design the core has a stiffness equal to κ_0 and a viscous damping element with a coefficient η in the vertical direction. When negative stiffness inclusions are incorporated and in order for the two designs to be statically equivalent, the vertical stiffness of the core is altered to κ_s (by altering its Young's modulus in the vertical direction) and an additional periodic branch is added comprising

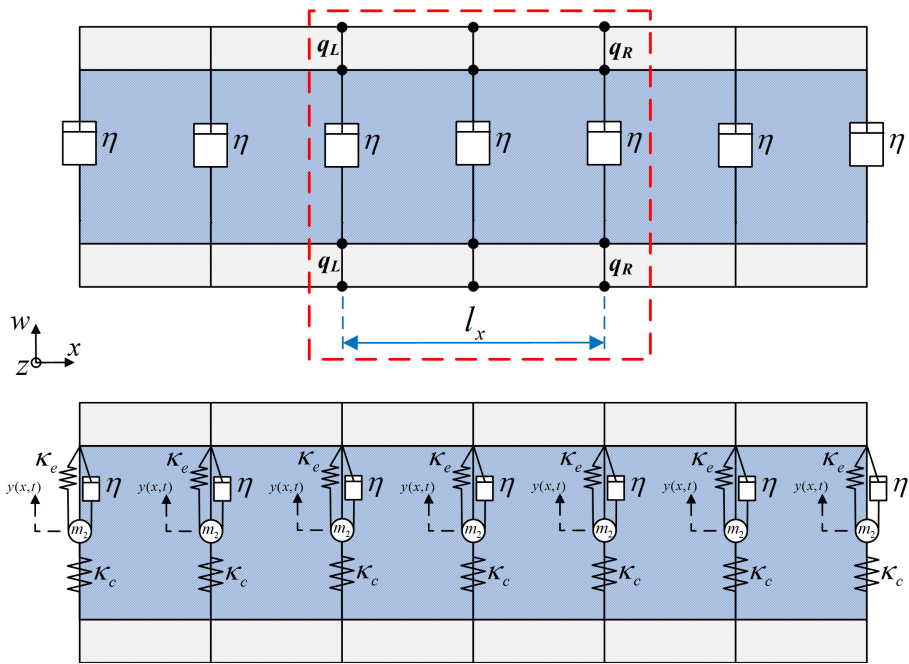


Figure 5: Illustration of an infinitesimal part of the considered layered beam. Dashed line encloses the considered periodic segment. Top: The structure with its facesheets connected to each other through a core having a longitudinal stiffness equal to κ_0 and a damping coefficient η . Bottom: The structure with its facesheets connected to each other through a core having a longitudinal stiffness equal to κ_s and the addition of the suggested mechanism with η equal to the precedent case, κ_e positive stiffness and κ_c negative stiffness elements.

the stiffness elements κ_e , κ_c as well as the viscous damping device of coefficient η . Both designs are illustrated in Fig.5.

As with the continuous beam structure, time harmonic wave propagation is considered within the layered beam in the x direction implying

$$w(x, \omega, t) = W e^{i(\omega t - kx)} \quad (23)$$

A clarification on the equivalence of Eq.16 and Eq.23 is presented in what follows.

4.1. A note on the equivalence of the two Bloch's theorem expressions

It is noted that Eq.23 assumes spatial wave dissipation in contrast to Eq.16 where time induced wave dissipation was considered. However the two expressions are totally equivalent implying

$$e^{i(\omega t - (k_{re} + ik_{im})x)} = e^{-ik_{re}x + (\lambda_{re} + i\lambda_{im})t} \quad (24)$$

Considering the wave propagation at a distance equal to one wavelength μ from the reference point which will inevitably correspond to one period T the above equivalence is expressed as

$$e^{i(\omega T - (k_{re} + ik_{im})\mu)} = e^{-ik_{re}\mu + (\lambda_{re} + i\lambda_{im})T} \Rightarrow e^{k_{im}\mu} = e^{\lambda_{re}T} \quad (25)$$

therefore $\lambda_{re}T = k_{im}\mu$, however $\mu = 2\pi/k_{re}$, $T = 2\pi/\omega$ and $\lambda_{re} = -\xi\omega$ therefore

$$\xi = -k_{im}/k_{re} \quad (26)$$

for a direct comparison between the two approaches of dissipation modelling.

4.2. Wave propagation properties

The problem will be modelled by a wave and finite element approach (coupling FE to periodic structure theory) as exhibited in [45]. The structure can be modelled using standard FE techniques and the Dynamic Stiffness Matrix (DSM)

$$\mathbf{D} = \mathbf{K} - \omega^2 \mathbf{M} + i\omega \mathbf{C} \quad (27)$$

can be calculated for each considered frequency. The DSM is subsequently partitioned with regard to its left/right sides and internal DoF as

$$\begin{bmatrix} \mathbf{D}_{LL} & \mathbf{D}_{LI} & \mathbf{D}_{LR} \\ \mathbf{D}_{IL} & \mathbf{D}_{II} & \mathbf{D}_{IR} \\ \mathbf{D}_{RL} & \mathbf{D}_{RI} & \mathbf{D}_{RR} \end{bmatrix} \begin{Bmatrix} \mathbf{q}_L \\ \mathbf{q}_I \\ \mathbf{q}_R \end{Bmatrix} = \begin{Bmatrix} \mathbf{f}_L \\ \mathbf{0} \\ \mathbf{f}_R \end{Bmatrix} \quad (28)$$

with \mathbf{q} the displacement and \mathbf{f} the force vectors. By condensing the internal DoF the problem can be expressed as

$$\begin{bmatrix} \mathbf{D}_{LL} - \mathbf{D}_{LI}\mathbf{D}_{II}^{-1}\mathbf{D}_{IL} & \mathbf{D}_{LR} - \mathbf{D}_{LI}\mathbf{D}_{II}^{-1}\mathbf{D}_{IR} \\ \mathbf{D}_{RL} - \mathbf{D}_{RI}\mathbf{D}_{II}^{-1}\mathbf{D}_{IL} & \mathbf{D}_{RR} - \mathbf{D}_{RI}\mathbf{D}_{II}^{-1}\mathbf{D}_{IR} \end{bmatrix} \begin{Bmatrix} \mathbf{q}_L \\ \mathbf{q}_R \end{Bmatrix} = \begin{Bmatrix} \mathbf{f}_L \\ \mathbf{f}_R \end{Bmatrix} \quad (29)$$

Assuming that no external forces are applied on the segment the displacement continuity and force equilibrium equations at the interface of two consecutive periodic segments r and $r + 1$ give

$$\begin{aligned} \mathbf{q}_L^{r+1} &= \mathbf{q}_R^r \\ \mathbf{f}_L^{r+1} &= -\mathbf{f}_R^r \end{aligned} \quad (30)$$

Using Eqs.(29),(30) the relation of the displacements and forces of the left and right sides of the segment can be written as

$$\begin{Bmatrix} \mathbf{q}_L^{r+1} \\ \mathbf{f}_L^{r+1} \end{Bmatrix} = \mathbf{T} \begin{Bmatrix} \mathbf{q}_L^r \\ \mathbf{f}_L^r \end{Bmatrix} \quad (31)$$

and the expression of the symplectic [46] transfer matrix \mathbf{T} can be written as

$$\mathbf{T} = \begin{bmatrix} \mathbf{D}_{11} & \mathbf{D}_{12} \\ \mathbf{D}_{21} & \mathbf{D}_{22} \end{bmatrix} \quad (32)$$

with

$$\begin{aligned} \mathbf{D}_{11} &= -(\mathbf{D}_{LR} - \mathbf{D}_{LI}\mathbf{D}_{II}^{-1}\mathbf{D}_{IR})^{-1}(\mathbf{D}_{LL} - \mathbf{D}_{LI}\mathbf{D}_{II}^{-1}\mathbf{D}_{IL}) \\ \mathbf{D}_{12} &= (\mathbf{D}_{LR} - \mathbf{D}_{LI}\mathbf{D}_{II}^{-1}\mathbf{D}_{IR})^{-1} \\ \mathbf{D}_{21} &= -\mathbf{D}_{RL} + \mathbf{D}_{RI}\mathbf{D}_{II}^{-1}\mathbf{D}_{IL} + (\mathbf{D}_{RR} - \mathbf{D}_{RI}\mathbf{D}_{II}^{-1}\mathbf{D}_{IR})(\mathbf{D}_{LR} - \mathbf{D}_{LI}\mathbf{D}_{II}^{-1}\mathbf{D}_{IR})^{-1}(\mathbf{D}_{LL} - \mathbf{D}_{LI}\mathbf{D}_{II}^{-1}\mathbf{D}_{IL}) \\ \mathbf{D}_{22} &= -(\mathbf{D}_{RR} - \mathbf{D}_{RI}\mathbf{D}_{II}^{-1}\mathbf{D}_{IR})(\mathbf{D}_{LR} - \mathbf{D}_{LI}\mathbf{D}_{II}^{-1}\mathbf{D}_{IR})^{-1} \end{aligned} \quad (33)$$

Free wave propagation is described by the eigenproblem

$$\gamma \begin{Bmatrix} \mathbf{q}_L^r \\ \mathbf{f}_L^r \end{Bmatrix} = \mathbf{T} \begin{Bmatrix} \mathbf{q}_L^r \\ \mathbf{f}_L^r \end{Bmatrix} \quad (34)$$

whose solution γ_j is related to the complex values of the structural wavenumber k_j by

$$k_j = -\frac{\ln(\gamma_j)}{il_x} \quad (35)$$

corresponding to wave type j , with l_x being the length of the periodic segment r . The real part of k_j indicates the spatial frequency of the wave, while the imaginary part indicates spatial wave dissipation.

4.3. Dynamic structural stability criterion

Including negative stiffness elements in the modelled configuration has the potential to induce structural dynamic instabilities, [47] even if the included negative stiffness oscillator is stable when standing alone. For this reason the computed solutions of the eigenproblem in Eq.34 have to be checked against stability criteria. Dynamic instability implies the existence of waves for which the power flow transport occurs with an exponentially increasing amplitude. The time-averaged energy crossing the junction between two elements of the periodic waveguide is given [48] by

$$\langle \mathbb{E} \rangle = \frac{1}{2} \text{Re}(\mathbf{f}_R^T \dot{\mathbf{q}}_R) = \frac{1}{2} \text{Re}(i\omega \mathbf{f}_R^T \mathbf{q}_R) \quad (36)$$

However due to the time harmonic motion assumption

$$\begin{aligned} \mathbf{q}_R &= \gamma \mathbf{q}_L \\ \mathbf{f}_R &= -\gamma \mathbf{f}_L \end{aligned} \quad (37)$$

therefore the time-averaged energy can be written as

$$\langle \mathbb{E} \rangle = \frac{1}{2} \text{Re}(-i\omega \gamma^2 \mathbf{f}_L^T \mathbf{q}_L) \quad (38)$$

For damped systems $\text{Im}(k_j) \neq 0$ and for the waves propagating towards the positive values of x the following is true

$$|\gamma_j^+| < 1 \quad (39)$$

For positive-propagating waves the value of $\langle \mathbb{E}_j \rangle$ should be negative, suggesting that their amplitude would be decreasing towards the direction of propagation. Moreover, $\langle \mathbb{E}_j \rangle$ and $\text{Im}(k_j)$ should be of same signs, suggesting that the power flow takes place towards the same direction as the decrease of the wave amplitude and implying the following dynamic stability criterion

$$\text{Im}(k_j) \langle \mathbb{E}_j \rangle \geq 0 \quad (40)$$

which should be true for every computed wave type j .

5. Numerical case studies

5.1. Continuous beam

A continuous 'beam on a floor' as illustrated in Fig.4 is hereby considered with $E=700$ MPa, $I = 10^{-5}$ m⁴ and $M=1$ kg/m while $\kappa_0=10^7$ N/m and $\eta=0.1$. The wavenumbers for the flexural waves propagating within the supported beam are initially sought for the two configurations presented in Sec.3. Real values for k are injected into Eq.18, 22 and the corresponding complex values of λ are computed. It is noted that a value of $\varepsilon = 3\%$ is used throughout the calculations presented below.

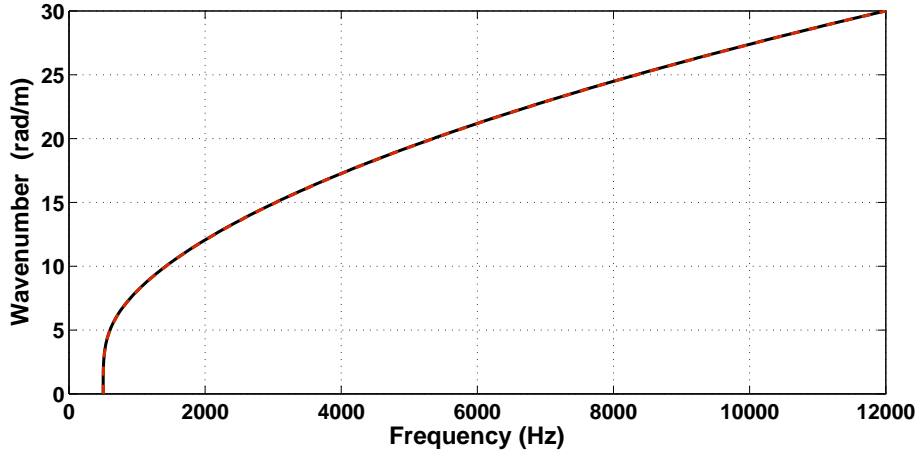


Figure 6: Wavenumber k as a function of frequency for the flexural wave propagating within the beam: No negative stiffness (—), With negative stiffness inclusions (---). Computations conducted with $\alpha=1.6$, $\eta=0.1$

5.1.1. Results for $m_2 = 0$

The results for the flexural wave propagating within the system when $m_2 = 0$ are exhibited in Fig.6. It can be observed that the effect of the inclusion of the suggested configuration with regard to the wave phase and group velocities is negligible throughout the considered frequency range. It is therefore evident that the two configurations are both statically and dynamically equivalent. A frequency band gap is also observed for the flexural wave within the 0-500 Hz region.

The damping ratio ξ for the flexural wave can be calculated through the real parts of λ . The results for the two configurations are presented in Fig.7. An impressive increase of the damping ratio by over three orders of magnitude is observed for the system having negative stiffness inclusions. Frequency dependence of ξ in this case is also observed with ξ presenting a slight decrease for higher frequencies. On the other hand, for the original system ξ remains constant with respect to frequency.

A parametric analysis with regard to η is subsequently conducted. The values of the damping ratios for three different values of η are presented in Fig.8. The damping coefficient is raised by an order of magnitude each time. For the original system it is observed that the increase of ξ is fairly proportional to the increase of η and no frequency dependence is observed as expected. With regard to the modified system, it is observed that ξ will gradually decrease, asymptotically converging towards the damping ratio of the original system at high frequencies. For the modified system, ξ also presents a trend to increase with η , however this increase is not proportional to the increment of η . This result is in accordance with the conclusions extracted from Fig.3. Once again, it is concluded that systems with lower inherent damping coefficient see more pronounced increases in their wave damping ratio ξ in the presence of the suggested oscillator.

All the above computations for the modified system were conducted using values for α that are optimal in terms of maximizing ξ . The question that directly arises is therefore how penalising would be the fact of not designing a system

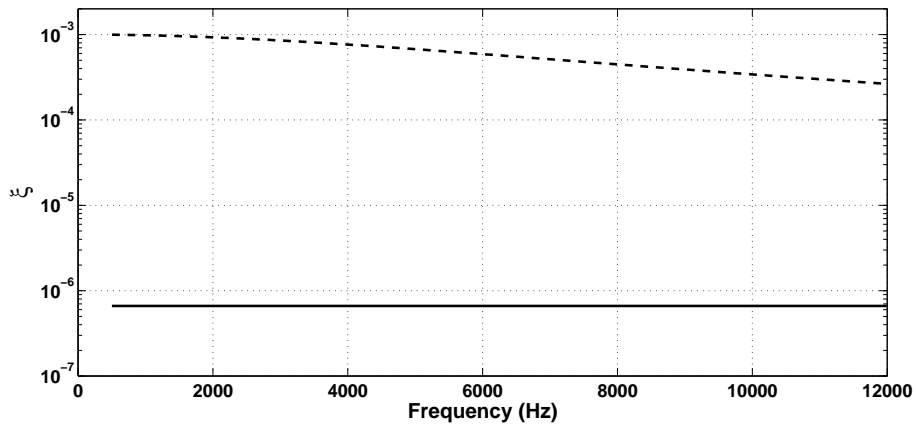


Figure 7: Damping ratio ξ as a function of frequency for the flexural wave propagating within the beam: No negative stiffness (—), With negative stiffness inclusions (---). Computations conducted with $\alpha=1.6$, $\eta=0.1$

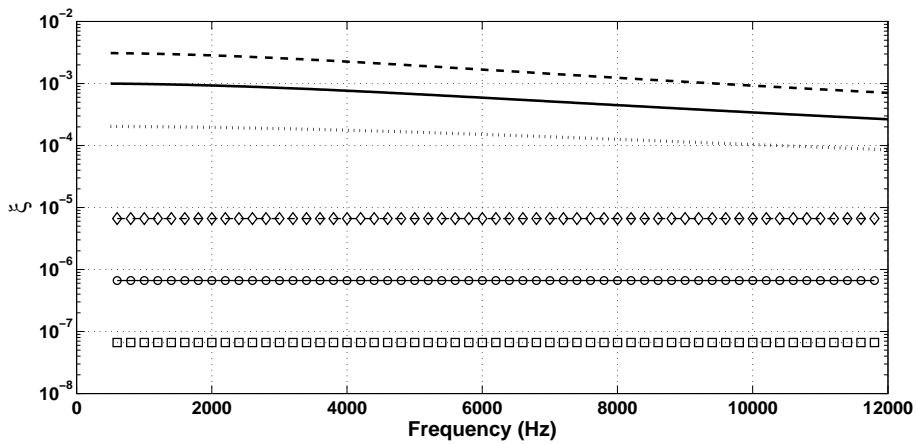


Figure 8: Damping ratio ξ as a function of frequency for the flexural wave propagating within the beam. Results for the SDoF oscillator: $\eta=0.01$ (\square), $\eta=0.1$ (\circ), $\eta=1$ (\diamond). Results for the mechanism having negative stiffness inclusions: $\eta=0.01$ and $\alpha=1.2$ (\cdots), $\eta=0.1$ and $\alpha=1.6$ (—), $\eta=1$ and $\alpha=3$ (---).

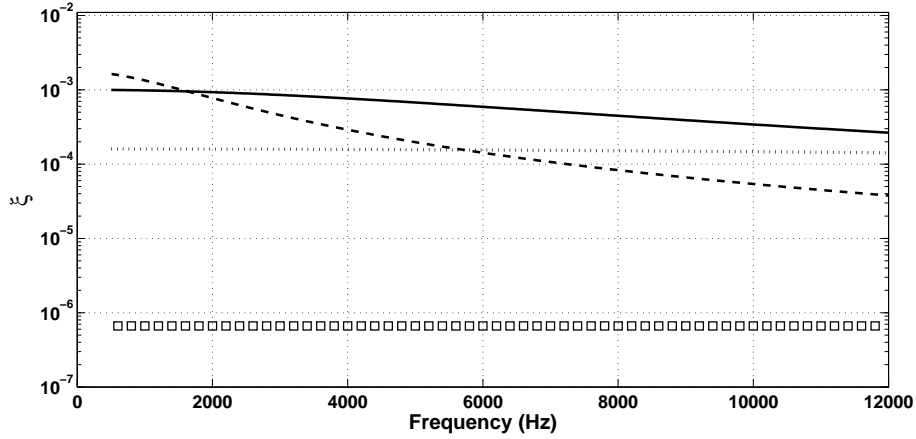


Figure 9: Damping ratio ξ as a function of frequency for the flexural wave propagating within the beam for $\eta=0.1$. Result for no negative stiffness (\square). Results for the mechanism having negative stiffness inclusions: $\alpha=1.3$ (- -), $\alpha=1.6$ (- · -), $\alpha=2.5$ (· · ·).

with an optimal α value. It is evident that for $\lim \alpha \rightarrow 1^+$ the system will converge towards the original configuration. Results for a below-optimal and an above-optimal value of α are presented in Fig.9. It is observed that for high values of α the system will generally exhibit reduced ξ values, while the frequency dependency of ξ is gradually alleviated. For higher values of α the resulting values of ξ will progressively be reduced and will converge towards the ones of the original system. For values of α below the optimal, the damping ratio presents a radical decrease for higher frequencies. For suboptimal α values however an increase of ξ is observed for very low frequencies.

5.1.2. Results for $m_2 > 0$

Results for $m_2 > 0$ are subsequently sought in order to investigate the effect of the added mass on the wavenumber and the damping ratio for the propagating waves. Three values for m_2 are introduced in the model

The results on the obtained values of k are presented in Fig.10. The first observation is related to the introduction of frequency band gaps due to the antiresonances induced by the designed oscillator. The frequency width of these band gaps increases with an increasing m_2 , while frequency-wise the band gaps occur at the antiresonance frequencies ω_a imposed by the design of the oscillator; with ω_a decreasing proportionally to $\sqrt{m_2}$.

The damping ratio of the propagating waves for various values of m_2 is presented in Fig.11. A maximum value for ξ is observed for $m_2 > 0$. This maximum occurs at the antiresonance frequency ω_a which varies in relation to the design of the configuration as described above. It is observed that for certain values of m_2 the maximum value of ξ can be even higher than the one for $m_2 = 0$. It is also shown that when $m_2 > 0$, in the high frequency range the value of ξ will converge towards the damping ratio of the SDoF oscillator. This convergence will be faster for systems having a larger m_2 . It is interesting to note that when a high damping ratio is desired within a specified frequency band, ω_a can be tailored for maximising ξ within that frequency range.

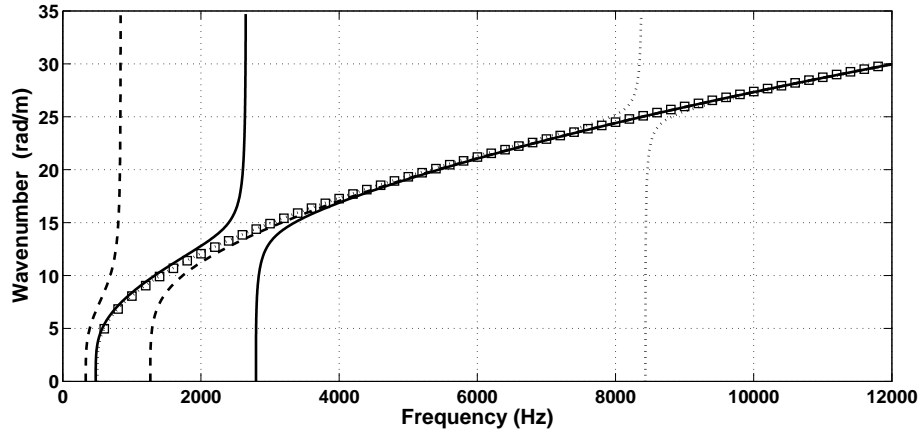


Figure 10: Wavenumber k as a function of frequency for the waves propagating within the beam. Result for no negative stiffness inclusions (\square). Results for various values of m_2 : $m_2=0.3M$ ($--$), $m_2=0.03M$ ($-$), $m_2=0.003M$ (\cdots). Computations conducted with $\alpha=3$, $\eta=0.1$

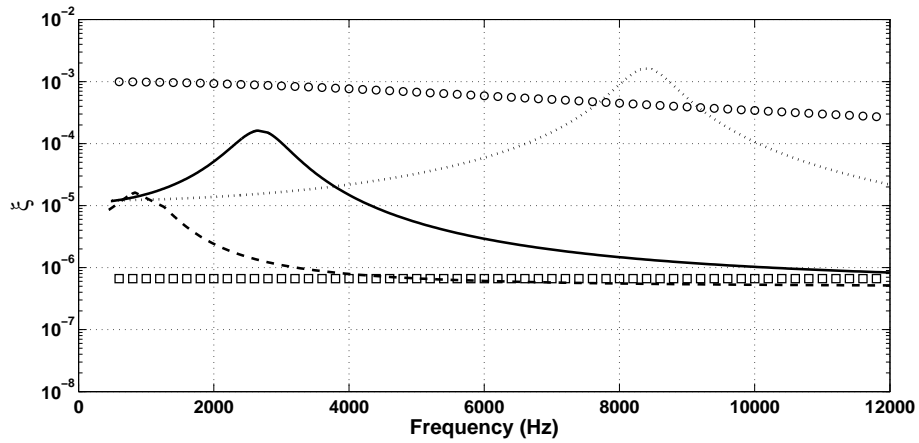


Figure 11: Damping ratio ξ as a function of frequency for the waves propagating within the beam for $\eta=0.1$. Result for no negative stiffness (\square) and modified configuration with $m_2=0$ (\circ). Results for: $m_2=0.3M$ ($--$), $m_2=0.03M$ ($-$), $m_2=0.003M$ (\cdots).

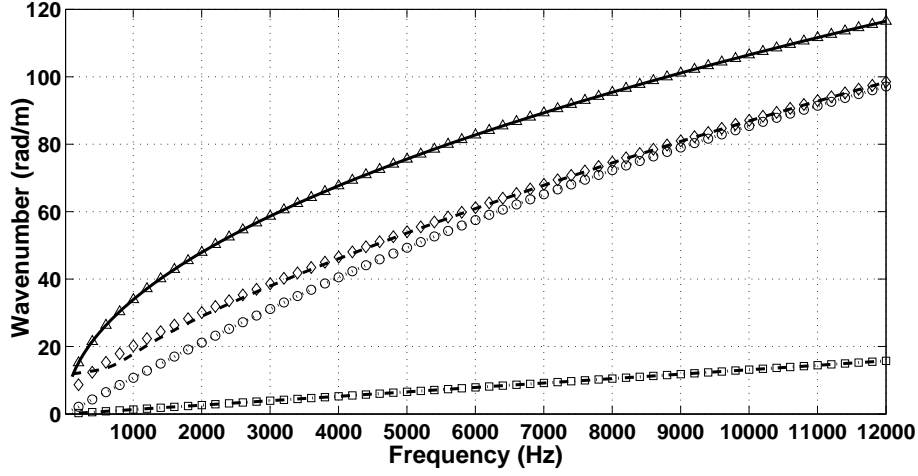


Figure 12: Real part of the wavenumbers for each wave type propagating within the layered beam. P-wave type: No negative stiffness (\square), With negative stiffness inclusions ($- \cdot -$). Torsional: No negative stiffness (\circ), With negative stiffness inclusions ($\cdot \cdot \cdot$). Bending around z axis: No negative stiffness (\diamond), With negative stiffness inclusions ($- \cdot -$). Bending around w axis: No negative stiffness (Δ), With negative stiffness inclusions ($-$).

5.2. Periodic layered beam

A layered beam is hereby modelled comprising two facesheets and a core layer. The facesheets are made of an isotropic material having a Young's modulus $E_f=70$ GPa, a Poisson's ratio $\nu_f=0.3$ and a mass density of $\rho_f=3000$ kg/m³. The thickness of the facesheets is equal to $h_f=1$ mm. The core has a thickness equal to $h_c=6$ mm and is made of a material having $E_c=0.7$ GPa, $\nu_c=0.2$ and $\rho_c=50$ kg/m³. The length of the period is $l_x = 5$ mm while the width of the beam is equal to 3 mm. It is noted that the parameter values $\varepsilon = 3\%$ and $\alpha = 2$ are used throughout the calculations presented below for the modified structure.

The layered structure is modelled through standard FE approaches. Matrices \mathbf{K} , \mathbf{M} and \mathbf{C} are computed and postprocessed as described in Sec.4.2 in order to obtain the acoustic wave propagation properties. All computations were conducted using the R2013a version of MATLAB[®].

5.2.1. Results for $m_2 = 0$

The real part of the wavenumbers for the four wave types propagating within the layered structure when $m_2 = 0$ is exhibited in Fig.12. An pronounced correlation between the results for the initial and the modified structure can be observed validating the assumption of the static equivalence of the two structures. For the out of plane flexural motion around axis z discrepancies are observed between the two configurations for very low frequencies, which are due to the impact of the high damping ratio of the flexural motion in this frequency range.

The ratio of the imaginary to the real part of the wavenumber for the flexural motion around z axis of the layered beam is exhibited in Fig.13. The quantity is equivalent to the damping ratio of the wave ξ . An inverse tendency is observed for the two quantities. While ξ is constantly increasing with respect to frequency for the initial system with

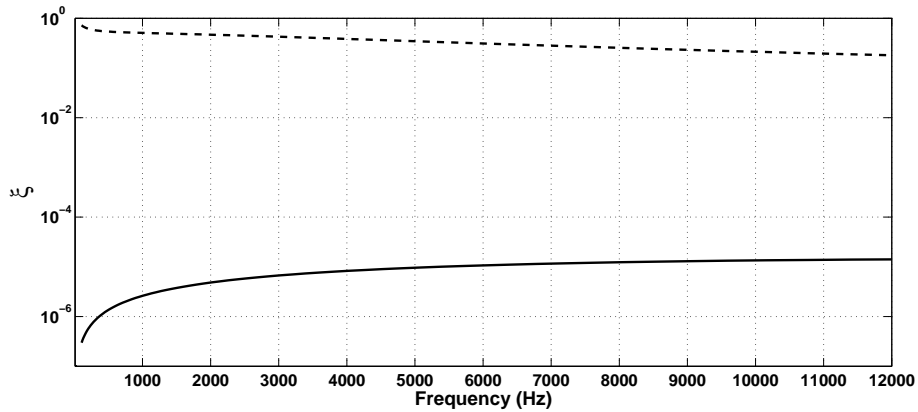


Figure 13: Damping ratio of the predicted flexural motion around z axis of the layered beam: No negative stiffness (-), Modified with negative stiffness inclusions (- -).

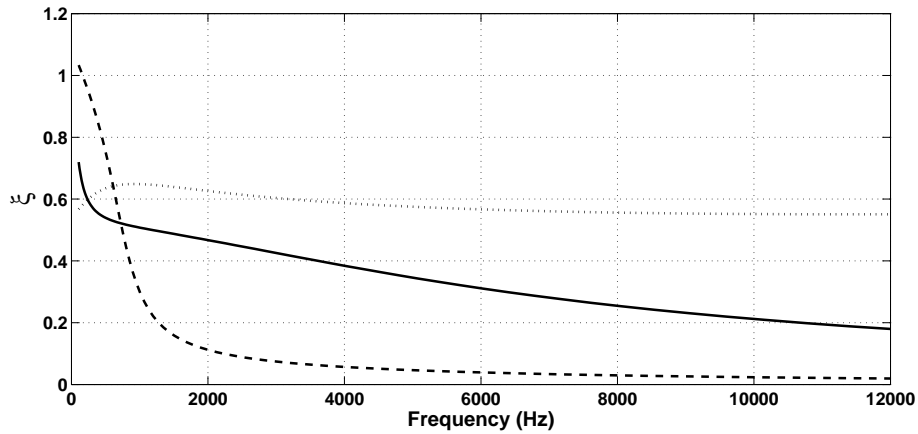


Figure 14: Damping ratio of the predicted flexural motion of the modified layered beam around z axis: With $\eta=10$ (\cdots), With $\eta=1$ (-), With $\eta=0.1$ (- -)

an asymptotic tendency, the damping ratio for the modified structure presents a constant decrease. A radical increase (more than six orders of magnitude) of ξ is observed in the very low frequency range, while at frequencies around 10 kHz this increase drops to approximately four orders of magnitude.

A parametric survey on the effect of the damping coefficient η on the damping ratio of the flexural motion around z axis of the layered beam is presented in Fig.14. It seems that lowering η will intensify the peak of ξ in the low frequency range. For higher frequencies the damping ratio quickly settles down towards an asymptotic limit; that is the damping ratio value of the unmodified structure. An effort on understanding the damping ratio frequency dependence and optimising the design of the oscillator for targeted frequency bands is ongoing. On the other hand, for an increased η value the low frequency peak of ξ is suppressed. An increase of one order of magnitude for η induces an approximately 550% increase of the damping ratio, confirming the conclusions drawn for the beam structure in Sec.5.

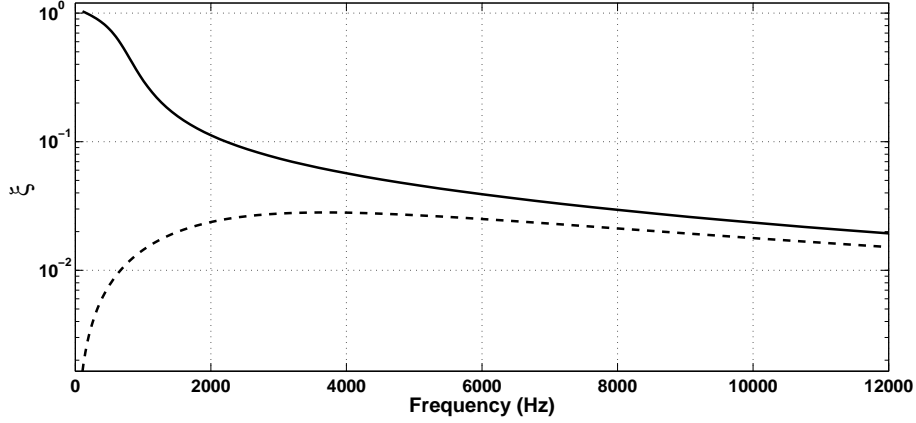


Figure 15: Damping ratio of the predicted flexural motion of the modified layered beam around z axis when $\eta=0.1$: With $m_2=0$ (—), With $m_2=0.3m_f$ (---)

5.2.2. Results for $m_2 > 0$

The values of the damping ratio for the flexural wave when $m_2 > 0$ are exhibited in Fig.15. The added lumped mass is expressed as a function of m_f which stands for the total mass of the facesheets included within one period of the modelled segment. The results present a maximum of ξ at the antiresonance frequency of the oscillator as was the case for the continuous beam structure. In the higher frequency range the damping ratio asymptotically converges towards the values obtained for the modified sandwich having $m_2 = 0$.

6. Conclusions

The main findings of the work are summarized as follows:

(i) The design of a configuration comprising negative stiffness elements was exhibited and implemented in continuous and periodic structures and the attenuation of the propagating waves was computed using analytical models as well as a wave and finite element approach.

(ii) The structural stability of both the oscillator and the modelled waveguides was discussed and ensured. A dynamic stability criterion for the waves propagating within the modelled structures was exhibited.

(iii) A radical increase of several orders of magnitude was exhibited for the damping ratio of the flexural waves propagating within the modelled configurations having negative stiffness inclusions.

(iv) It was shown that the added mass implied by the adoption of the modified oscillator can be designed for maximising the damping ratio of the system within a targeted frequency range.

(v) It was demonstrated that the damping ratio increase due to the inclusion of the suggested mechanism will be greater for lightly damped systems.

This work has shown how a lumped parameter oscillator can be used within periodic structures in order to enhance their damping performance. The suggested oscillator has simultaneous high stiffness and damping properties and

extends the existing concepts concerning single DoF negative stiffness and zero-stiffness oscillators. Future work will focus on manufacturing and implementing the suggested configuration within continuous systems in order to compare their performance to high damping/stiffness composite materials exhibited in recent bibliography.

References

- [1] E. Rivin, *Passive vibration isolation*, ASME Press New York, 2003.
- [2] J. M. Kelly, D. Konstantinidis, *Mechanics of rubber bearings for seismic and vibration isolation*, John Wiley & Sons, 2011.
- [3] Y. Wang, M. Ludwigson, R. Lakes, Deformation of extreme viscoelastic metals and composites, *Materials Science and Engineering: A* 370 (2004) 41–9.
- [4] P. Shorter, Wave propagation and damping in linear viscoelastic laminates, *The Journal of the Acoustical Society of America* 115 (2004) 1917–25.
- [5] E. Manconi, B. R. Mace, Estimation of the loss factor of viscoelastic laminated panels from finite element analysis, *Journal of Sound and Vibration* 329 (2010) 3928–39.
- [6] R. Lakes, Extreme damping in composite materials with a negative stiffness phase, *Physical Review Letters* 86 (2001) 2897–8.
- [7] T. Jaglinski, D. Kochmann, D. Stone, R. Lakes, Composite materials with viscoelastic stiffness greater than diamond, *Science* 315 (2007) 620–2.
- [8] R. Ibrahim, Recent advances in nonlinear passive vibration isolators, *Journal of Sound and Vibration* 314 (2008) 371–452.
- [9] C. S. Wojnar, D. M. Kochmann, A negative-stiffness phase in elastic composites can produce stable extreme effective dynamic but not static stiffness, *Philosophical Magazine* 94 (2014) 532–55.
- [10] C. S. Wojnar, D. M. Kochmann, Stability of extreme static and dynamic bulk moduli of an elastic two-phase composite due to a non-positive-definite phase, *physica status solidi (b)* 251 (2014) 397–405.
- [11] K. Virk, A. Monti, T. Trehard, M. Marsh, K. Hazra, K. Boba, C. Remillat, F. Scarpa, I. Farrow, SILICOMB PEEK Kirigami cellular structures: mechanical response and energy dissipation through zero and negative stiffness, *Smart Materials and Structures* 22 (2013) 084014–.
- [12] E. Baravelli, M. Ruzzene, Internally resonating lattices for bandgap generation and low-frequency vibration control, *Journal of Sound and Vibration* 332 (2013) 6562–79.
- [13] P. Michelis, V. Spitas, Numerical and experimental analysis of a triangular auxetic core made of CFR-PEEK using the Directionally Reinforced Integrated Single-yarn (DIRIS) architecture, *Composites Science and Technology* 70 (2010) 1064–71.
- [14] T. Klatt, M. R. Haberman, A nonlinear negative stiffness metamaterial unit cell and small-on-large multiscale material model, *Journal of Applied Physics* 114 (2013).
- [15] E. Pasternak, A. V. Dyskin, G. Sevel, Chains of oscillators with negative stiffness elements, *Journal of Sound and Vibration* 333 (2014) 6676–87.
- [16] R. Lakes, P. Rosakis, A. Ruina, Microbuckling instability in elastomeric cellular solids, *Journal of Materials Science* 28 (1993) 4667–72.
- [17] V. Spitas, C. Spitas, P. Michelis, Modeling of the elastic damping response of a carbon nanotube–polymer nanocomposite in the stress-strain domain using an elastic energy release approach based on stick-slip, *Mechanics of Advanced Materials and Structures* 20 (2013) 791–800.
- [18] L. Dong, R. Lakes, Advanced damper with high stiffness and high hysteresis damping based on negative structural stiffness, *International Journal of Solids and Structures* 50 (2013) 2416–23.
- [19] W. Molyneaux, *Supports for vibration isolation*, ARC/CP-322, Aeronautical Research Council, Great Britain, 1957.
- [20] P. Alabuzhev, E. I. Rivin, *Vibration protection and measuring systems with quasi-zero stiffness*, CRC Press, 1989.
- [21] D. L. Platus, Negative-stiffness-mechanism vibration isolation systems, In: *SPIE’s International Symposium on Optical Science, Engineering, and Instrumentation* (1999) 98–105.
- [22] J. Winterflood, D. Blair, B. Slagmolen, High performance vibration isolation using springs in euler column buckling mode, *Physics Letters A* 300 (2002) 122–30.

- [23] L. Virgin, R. Davis, Vibration isolation using buckled struts, *Journal of Sound and Vibration* 260 (2003) 965–73.
- [24] R. Plaut, J. Sidbury, L. Virgin, Analysis of buckled and pre-bent fixed-end columns used as vibration isolators, *Journal of Sound and Vibration* 283 (2005) 1216–28.
- [25] L. Virgin, S. Santillan, R. Plaut, Vibration isolation using extreme geometric nonlinearity, *Journal of Sound and Vibration* 315 (2008) 721–31.
- [26] R. DeSalvo, Passive, nonlinear, mechanical structures for seismic attenuation, *Journal of Computational and Nonlinear Dynamics* 2 (2007) 290–8.
- [27] B. A. Fulcher, D. W. Shahan, M. R. Haberman, C. C. Seepersad, P. S. Wilson, Analytical and experimental investigation of buckled beams as negative stiffness elements for passive vibration and shock isolation systems, *Journal of Vibration and Acoustics* 136 (2014).
- [28] A. Carrella, M. Brennan, T. Waters, Static analysis of a passive vibration isolator with quasi-zero-stiffness characteristic, *Journal of Sound and Vibration* 301 (2007) 678–89.
- [29] H. Huang, C. Sun, G. Huang, On the negative effective mass density in acoustic metamaterials, *International Journal of Engineering Science* 47 (2009) 610–7.
- [30] C.-M. Lee, V. Goverdovskiy, A. Temnikov, Design of springs with negative stiffness to improve vehicle driver vibration isolation, *Journal of Sound and Vibration* 302 (2007) 865–74.
- [31] T. D. Le, K. K. Ahn, A vibration isolation system in low frequency excitation region using negative stiffness structure for vehicle seat, *Journal of Sound and Vibration* 330 (2011) 6311–35.
- [32] C.-M. Lee, V. Goverdovskiy, A multi-stage high-speed railroad vibration isolation system with negative stiffness, *Journal of Sound and Vibration* 331 (2012) 914–21.
- [33] H. Iemura, M. H. Pradono, Advances in the development of pseudo-negative-stiffness dampers for seismic response control, *Structural Control and Health Monitoring* 16 (2009) 784–99.
- [34] A. A. Sarlis, D. T. R. Pasala, M. Constantinou, A. Reinhorn, S. Nagarajaiah, D. Taylor, Negative stiffness device for seismic protection of structures, *Journal of Structural Engineering* 139 (2012) 1124–33.
- [35] C.-M. Lee, V. Goverdovskiy, S. Samoilenko, Prediction of non-chaotic motion of the elastic system with small stiffness, *Journal of Sound and Vibration* 272 (2004) 643–55.
- [36] A. Carrella, M. Brennan, T. Waters, V. Lopes Jr, Force and displacement transmissibility of a nonlinear isolator with high-static-low-dynamic-stiffness, *International Journal of Mechanical Sciences* 55 (2012) 22–9.
- [37] I. Kovacic, M. J. Brennan, T. P. Waters, A study of a nonlinear vibration isolator with a quasi-zero stiffness characteristic, *Journal of Sound and Vibration* 315 (2008) 700–11.
- [38] A. Shaw, S. Neild, D. Wagg, Dynamic analysis of high static low dynamic stiffness vibration isolation mounts, *Journal of Sound and Vibration* 332 (2013) 1437–55.
- [39] X. Huang, X. Liu, J. Sun, Z. Zhang, H. Hua, Vibration isolation characteristics of a nonlinear isolator using euler buckled beam as negative stiffness corrector: A theoretical and experimental study, *Journal of Sound and Vibration* 333 (2014) 1132–48.
- [40] B. Budiansky, Theory of buckling and post-buckling behavior of elastic structures, *Advances in applied mechanics* 14 (1974) 1–65.
- [41] S. Livet, M. Collet, M. Berthillier, P. Jean, J.-M. Cote, Structural multi-modal damping by optimizing shunted piezoelectric transducers, *European Journal of Computational Mechanics/Revue Européenne de Mécanique Numérique* 20 (2011) 73–102.
- [42] Y.-C. Wang, R. S. Lakes, Stable extremely-high-damping discrete viscoelastic systems due to negative stiffness elements, *Applied physics letters* 84 (2004) 4451–3.
- [43] F. Bloch, Über die quantenmechanik der elektronen in kristallgittern, *Zeitschrift für physik* 52 (1929) 555–600.
- [44] B. R. Mace, E. Manconi, Modelling wave propagation in two-dimensional structures using finite element analysis, *Journal of Sound and Vibration* 318 (2008) 884–902.
- [45] B. R. Mace, D. Duhamel, M. J. Brennan, L. Hinke, Finite element prediction of wave motion in structural waveguides, *The Journal of the Acoustical Society of America* 117 (2005) 2835–43.
- [46] W. Zhong, F. Williams, On the direct solution of wave propagation for repetitive structures, *Journal of Sound and Vibration* 181 (1995)

485–501.

- [47] M. Collet, K. A. Cunefare, M. N. Ichchou, Wave motion optimization in periodically distributed shunted piezocomposite beam structures, *Journal of Intelligent Material Systems and Structures* (2008).
- [48] D. Mead, A general theory of harmonic wave propagation in linear periodic systems with multiple coupling, *Journal of Sound and Vibration* 27 (1973) 235–60.

List of symbols

b_i, c_i	Coefficient i of the characteristic equation
E	Young's modulus
$\langle E \rangle$	Time averaged wave energy
f	External force
I	Second moment of area
l	Length of the periodic segment
m, M	Mass variables
s	Laplace variable
w	Apparent DoF
y	Internal DoF
C	Damping matrix
D	Dynamic stiffness matrix
K	Stiffness matrix
M	Mass matrix
T	Transfer matrix
q	Displacement DoF vector
f	Force vector
γ	Transfer matrix eigenvalue
ε, α	Design parameters of the oscillator
ζ	Damping ratio of the oscillator's motion
η	Damping coefficient
$\kappa_0, \kappa_s, \kappa_e$	Positive stiffnesses
κ_c	Negative stiffness
λ	Complex frequency function
μ	Wavelength
ξ	Wave damping ratio
ω	Angular frequency